Screener3D: a Gaseous Time Projection Chamber for Ultra-low Radioactive Material Screening

Haiyan Du,¹ Chengbo Du,² Karl Giboni,¹ Ke Han,^{1,*} Shengming He,² Liqiang Liu,² Yue Meng,¹ Shaobo Wang,^{1,3} Tao Zhang,¹ Li Zhao,¹ and Jifang Zhou²

¹INPAC; Shanghai Laboratory for Particle Physics and Cosmology; Key Laboratory for Particle Astrophysics and Cosmology (MOE),
School of Physics and Astronomy, Shanghai Jiao Tong University, Shanghai 200240, China

²Yalong River Hydropower Development Company, Ltd., 288 Shuanglin Road, Chengdu 610051, China

³SPEIT (SJTU-ParisTech Elite Institute of Technology),
Shanghai Jiao Tong University, Shanghai, 200240, China

For experiments searching for rare signals, background events from the detector itself are one of the major limiting factors for search sensitivity. Screening for ultra-low radioactive detector material is becoming ever more essential. We propose to develop a gaseous Time Projection Chamber (TPC) with Micromegas readout for radio-screening purposes. The TPC records three-dimensional trajectories of charged particles emitted from a flat sample placed inside the active volume. The detector is able to distinguish the origin of an event and identify the particle types with information from trajectories, which improves the screening sensitivity significantly. For α particles from the sample surface, we find that our proposed detector can reach a sensitivity of better than $100~\mu \mathrm{Bq \cdot m^{-2}}$ within two days.

Keywords: Charged Particle detector, surface α measurement, Ultra-low Radioactive, Material Screening

I. INTRODUCTION

Experiments searching for neutrinoless double beta decay [1] and dark matter direct detection signals [2, 3] have extremely low signal rate, if not null at all. The background rate recorded by the detector is essential to search sensitivities. In underground laboratories such as China Jinping Underground Laboratory (CJPL) [4], the influence of cosmic rays is reduced by orders of magnitude and no longer dominant. Background events are almost entirely from the detector itself and the surrounding lab environment. Therefore, extensive material screening campaigns to select materials with low radioactivities have been carried out by many experiments (for example, refer to [5–10]). The majority of the efforts emphasize bulk radioactivities of materials using screening techniques such as γ -ray measurement with high purity germanium (HPGe) detectors.

Surface radioactivities are often much different from those in the bulk and may contribute significantly to the background budget. The surface of detector components may get contaminated with additional radioactivities by machining, handling, or just exposing to air. When facing directly to a detector's active volume, α or β particles emitted from the surface may introduce background events directly. The surface background is especially critical for modular detectors where large surface areas facing detector modules. For example, α events from detectors' supporting structure and detector surface are the most prominent source in the CUORE bolometer array [11]. Even if surface contaminations are far from detectors, radioactive impurities may emanate from the surface and travel to the detector via circulation of liquid or gas detector medium. Take the PandaX-4T experiment as an example, ²²²Rn from detector and circulation pipe's inner surface is a major background source for the dark matter search [12].

Surface radioactivities are often measured with semiconductor detectors, scintillator arrays, gas ionization counters, etc. The detection areas of commercial silicon semiconductor detectors are usually smaller than 100 cm² (e.g. [13]. An example scintillator array is BiPo-3, which utilizes 40 scintillator modules for a total screening area of 3.6 m² [14]. The extremely sensitive detector does require dedicated support and therefore cost for measurement is high. Gas ionization counters can have large active areas and particle identification capability with pulse shape analysis. Ultralo 1800 offered by XIA [15] is one such detector. However, it does not take full advantage of the three-dimensional track recording capabilities of gas detectors. Proposals such as BetaCage [16] and gaseous detector with micro-time-projection chamber [17] are no longer active or in the early stage of development.

We propose to construct a low background gaseous Time Projection Chamber (TPC) to measure surface contaminations, which we call Screener3D. Screener3D will be able to measure energy and trajectories of α and β particles with position-sensitive Micromegas [18] (Micro-MEsh Gaseous Structure) readout modules. In a typical argon TPC operating at atmospheric pressure, α particles of 10 MeV travel approximately 10 cm in an almost straight line. Trajectories of β particles of the same energy are much longer and meandering. Along the particle trajectories, the gas medium is ionized. The number and initial position of ionization electrons carry the three-dimensional trajectory information of the original particle. When combining energy and trajectory information, we can better distinguish signals from the background and identify the origin of the signals. Samples will be placed in the TPC and the emitted charged particles are recorded with high efficiency. Especially for α particle, the energy can be measured more accurately without energy loss in entrance windows. The cost of gaseous detectors is relatively low for a large measured area, which further improves the measurement efficiency and shortens the measuring time. In this paper, we give an overview of the proposed design and sensitivity studies with simulation.

^{*} Corresponding author, ke.han@sjtu.edu.cn

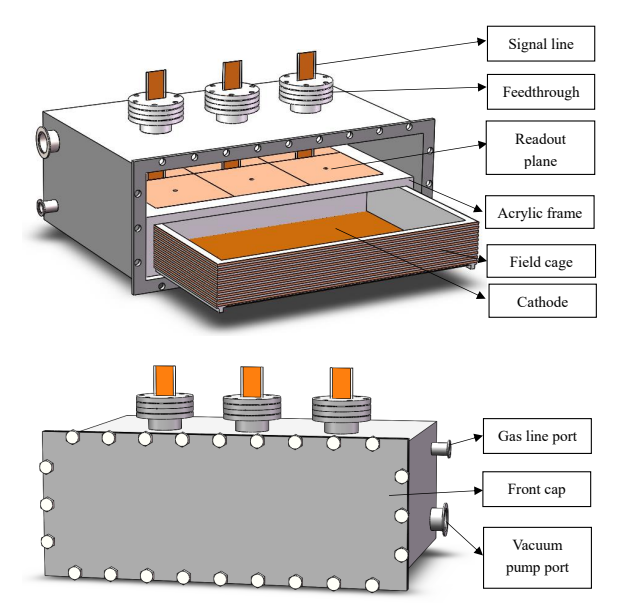


Fig. 1. Schematic design of Screener3D with main components labeled. (Top) The inside view with field cage drawer pulled out. Samples are placed at the bottom of the drawer (on the cathode). (Bottom) The detector with front cap closed and ready for measurement.

II. DESIGN OVERVIEW

The central part of Screener3D is the low-background, large-area, and high-granularity gaseous TPC. All the materials used to build the TPC will be of low radioactivities to control the background contributions from the detector itself. The designed readout area, which determines the largest sample area that can be measured, is about 2000 cm². The Micromegas readout will be based on 3 mm wide strips, a granularity enough for α and β tracks on the order of 10 cm. Besides the key detector performance specifications, Screener3D must be stable over an extended period. The long-term stability is maintained with a gas circulation and purification system and a real-time monitoring system. With the auxiliary systems, we can measure samples for a prolonged period of up to weeks to improve the measurement sensitivity. We will describe the main components of Screener3D and material screening plans in this section.

A. Gaseous TPC with Micromegas

The Screener3D TPC mainly comprises a readout plane with Micromegas modules, a cathode, a field cage, a gas medium, and an outer vessel, as illustrated in Fig. 1. The rectangular readout plane on the top is for collecting drift electrons after amplification via avalanche. The cathode is at the bottom and provides a negative high voltage. The field cage connects the readout plane and cathode mechanically and helps maintain a uniform drift electric field in the active volume, which is the cuboid space enclosed by the aforementioned components. The active volume is 60 cm long, 40 cm

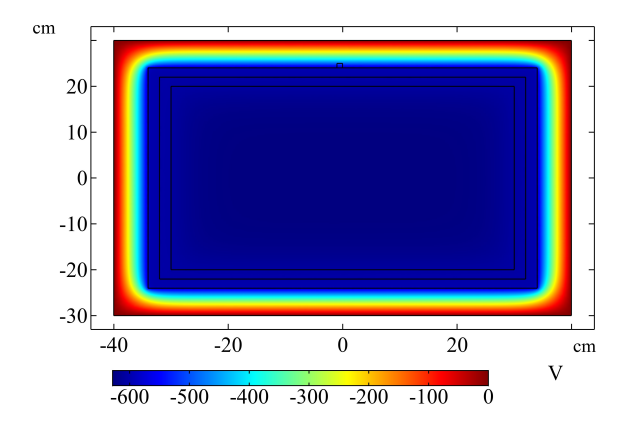
wide, and 10 cm high, which is filled with 1 bar of argon and isobutane gas mixtrue during operation. All the components are fixed inside the vessel with signal feedthroughs as well as various ports for gas circulation and pumping.

During measurement, a thin slab sample, such as a sheet of metal, plastic films, or silicon wafer, would be placed on the cathode plane. Radioactive contaminations on the top surface of the sample emit α and β particles into the active volume. We focus mainly on the identification of α particles from samples since the energy deposition in the unit distance is large and trajectory characteristics are easier to define. The typical α emissions are from uranium and thorium decay chains. Nuclide such as $^{232}{\rm Th},\,^{238}{\rm U},\,^{214}{\rm Po},\,$ and $^{212}{\rm Po}$ emit α particles with energy of 4.0, 4.1, 7.7, and 8.8 MeV respectively. A few other isotopes along the decay chains emit α particles in the energy range of 3 to 9 MeV.

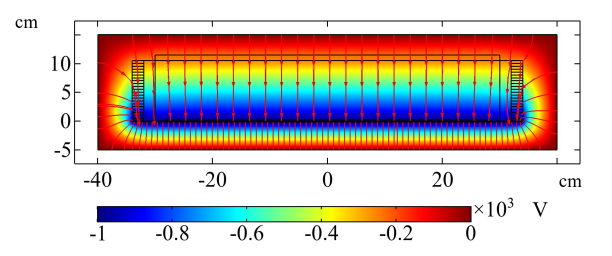
The readout plane may consist of multiple Micromegas modules. In our current design, 6 pieces of about $20 \times 20 \text{ cm}^2$ modules are tiled together to form a total readout area of 2400 cm². In Fig. 1, the modules are shown face-down, supported by an acrylic frame. For each module, the active area is split into 64×64 diamond-shaped pads, each of which has a diagonal length of 3 mm. The pads are inter-connected in vertical or horizontal direction and form the so-called X or Y readout strips. With 64 X strips and 64 Y strips, the total number of electronics channels is 128 per module. Flat signal cables made of Kapton-based flexible print circuit board (PCB) pass through the feedthroughs on the top of the vessel to send the signals to readout electronics (not shown in the figure) outside the TPC. Micromegas modules are usually biased at a few hundreds of volts and the voltage is provided through the flat Kapton cable as well.

Fig. 1 (top) also shows the field cage and cathode as a drawer pulled out from the acrylic frame. The sidewall of the field cage is made of 2 cm thick acrylic plates with Kaptonbased flexible PCB attached to the outside. There are uniformly spaced copper strips on the PCB and the adjacent strips are connected with surface mount resistors. At the bottom of the drawer, a polished copper plate of 0.2 cm thickness is used as the cathode. The cathode is electrically connected to the bottom strip of the field cage PCB. A uniform electric field is formed within the field cage when a negative high voltage is provided to the cathode. The whole setup is enclosed in an outer vessel made of 1 cm thick stainless steel (SS). To work with the drawer style field cage for easy sample loading, the opening of the vessel is at the front, as shown in Fig. 1 (bottom). Ports for gas lines, vacuum pump, and feedthrough for cathode high voltage cable are added on the side of the vessel.

Samples are placed on the cathode for measurement. In our current design shown in Fig. 1, the front panel of the vessel is unmounted, the field cage is pulled out, and then the sample can be placed on the cathode. Once closed again, we pump down the vessel roughly before flushing argon gas in. We expect the entire sample loading process to be done in the time frame of an hour. Alternative designs, such as a stationary field cage with a slit opening on the front, are also under consideration to further streamline the sample loading process.



(a) Top view of the detector showing potential on the XY plane



(b) Side view of the detector showing potential on the XZ plane

Fig. 2. Electric field simulation with COMSOL, which demonstrates minimal impact to electric field of samples on cathode. (a) Top view of the detector showing potential on the XY plane. The innermost black rectangle shows the boundary of the sample, which has a slightly smaller footprint than the active volume of the TPC. (b) Side view of the detector showing potential on the XZ plane. Red lines with arrows indicate the electric field lines. We can see the field lines are in almost perfect vertical directions above the sample's footprint.

When samples are placed in the active volume, the counting efficiency is high and the measurement of α -particle energy more accurate. One may concern about the disturbance of electric potential lines when samples are on the cathode. We simulate the effect of a thin Kapton sample with the COMSOL Multiphysics finite element analysis software [19] as shown in Fig 2. The black wireframes in Fig. 2 represent the internal structure of the TPC, such as the field cage, cathode, and readout modules. We supply the cathode with 1 kV negative voltage, and the readout plane 250 V negative voltage. The Kapton sample of 54.4 cm long, 34.4 cm wide, and 0.1 cm thick is shown as the innermost rectangle in Fig. 2 (a). Fig. 2 (b) shows the side view of field cage. The field lines inside the field cage show minimal distortions. In the X-Z plane, the electric field in the X direction is 3.6% of that in the vertical Z direction at 2 mm from the edge of the sample, while the value will be less than 1% at 2 cm from the edge of the sample. The uniformity of the electric field is almost the same for a copper or silicon sample of the same size and thus negligible for our measurement.

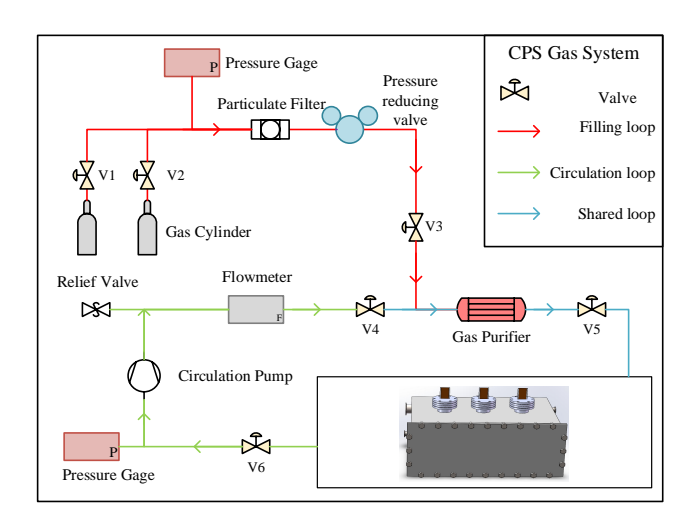


Fig. 3. Schematic diagram of the Screener3D gas system. Red arrows denote the filling loop. Green arrows denote the circulation loop. Blue arrows are for the loops shared by filling and circulation. After the pressure-reducing valve, the working pressure is limited to 1 bar.

B. Gas system and slow monitoring system

The energy response and resolution of gaseous TPC are highly sensitive to the purity of gas medium, especially electronegative impurities such as oxygen and water. The impurities may attract and absorb drift electrons in the active volume. They may also reduce the gain in the avalanche gap of Micromegas. For the stability of the prolonged measurement period of Screener3D, a gas circulation and purification system (shown in Fig. 3) are designed. Before flowing into the TPC, gas mixtures travels through a set of gas purifier. Given the different precision requirements of measurement, the purifier may be a charcoal-based absorber (mainly for absorbing radio-impurities such as radon), a chemical-reaction-based getter (mainly for absorbing electronegative impurities), or a combination of both. A circulation loop is added for continuous purification of working gas for extended measurement of low radioactivities samples.

To quantify the long-term (in)stability of the detector, we monitor key operation parameters, such as ambient temperature, detector temperature, gas pressure, Micromegas bias voltage, leakage current, TPC drift voltage, event rates, etc. We design and build a centralized Slow Monitoring System [20] (SMS) with all the parameter values stored in a database, and accessible in real-time in a web browser. With pre-defined safety ranges of key parameters, the SMS can also send alerts via email or phone text message. The SMS data also would enable us to reject or correct poor-quality data based on the variation of operating conditions. The SMS system may also store sample information, such as area, material, and screening time to serve as a centralized catalog of measurements.

C. Intrinsic background sources and mitigation

To improve the signal-to-background ratio in screening, radioactive background from Screener3D itself will be minimized. The inner part of Screener3D TPC will be built with materials of low radioactivity, screened with HPGe and/or mass spectrometer techniques. The cathode will be made with high-purity oxygen-free copper especially screened for low uranium and thorium contaminations. The field cage is designed to have only low-radioactivity acrylic facing the active volume to avoid background events from PCB and resistors. Surface contaminations of Micromegas are more challenging to measure and control. We used Microbulk Micromegas [18] in this study, which is made with Kapton and copper using PCB lithography technique and has been shown to have good performance and low surface radioactivities[21]. Furthermore, the surfaces of detector components, particularly those facing the active volume of the TPC, will be thoroughly cleaned to reduce the emission of α particles. The inner volume of the Screener3D will be filled or flushed with argon gas all the time to avoid radon contamination from the air. In our sensitivity study later, we assume all the detector components are made with low-radioactivity materials and no secondary surface contaminations are introduced in construction.

In addition to minimizing the radioactive emission from detector components, we can further suppress the background with topological information from particle tracks, which is the key feature of Screener3D. Tracks of α particles from a sample and various TPC components are illustrated in Fig. 4. The high energy α tracks are mostly straight in 1 bar of argon. A large blob at one end of the track is to highlight the dE/dxincrease when α particles stop. α events originated from the sample would have starting points from the sample surface and an upward-going direction in our detector geometry. For the contaminations of the field cage, α tracks enter the active volume from the side and may go upward or downward. Surface α events from the readout plane point downward and can be easily distinguished from those of the samples. During sample measurement, the majority of the surface area of the cathode is covered by a sample and no α particle from the cathode could enter the active volume excepted the very edge, as shown in the illustration. With the distinguished track features, we can greatly suppress α background from the detector and achieve a higher sensitivity. In the following section, we will demonstrate the suppression power with simulation data.

III. EXPECTED SCREENING SENSITIVITY

The screening sensitivity of Screener3D depends on the background event rates recorded by the detector. In this section, we set up a detector model in the simulation framework Geant4 [22], and describe major background sources for α particle measurement. The energy deposition process and gaseous detector response are implemented in the simulation. Signal selection and background suppression efficiencies are calculated firstly with energy cuts and particle identification.

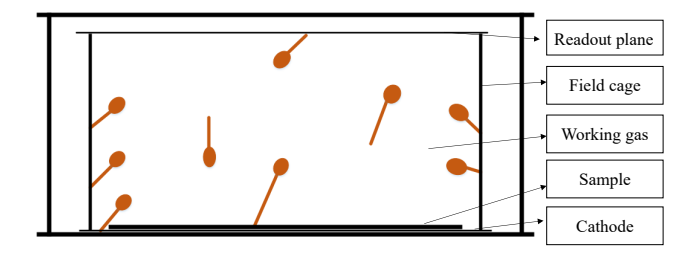


Fig. 4. illustration of α particles' trajectories in a gaseous TPC. α particles travel mostly in a straight line in 1 bar of argon and 5% isobutane gas with a prominent Bragg peak at the end. We utilize this feature for background suppression in our detector.

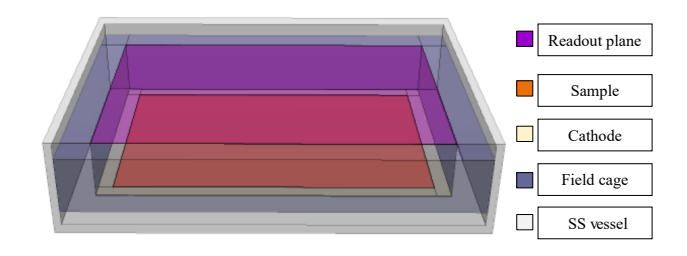


Fig. 5. The geometry of main components of Screener3D as constructed in the Geant4 simulation. All the dimensions follow the schematic design as shown in Fig. 1.

The unique tracking capability of the gaseous detector is then exploited to distinguish α particles from different origins and with different orientations to further reduce α background rate. We finally present the material screening sensitivity for surface contamination of α emitting impurities.

A. Screener3D background

Fig. 5 shows the detector geometry constructed in the Geant4 simulation [22]. The setup consists of the sensitive volume, field cage, readout plane, cathode, and SS vessel with dimensions identical to the detector's conceptual design. The sensitive volume in the center is a $60 \times 40 \times 10$ cm³ cuboid with 1 bar argon and 5% isobutane mixture. The readout plane is expected to be instrumented with Microbulk Micromegas, which has complicated mechanical structures, such

Table 1. Radioactivity level of bulk material in Screener3D $(mBq \cdot kg^{-1})$

Material	Gaseous	Acrylic	Oxygen-free	Stainless
	argon		copper	steel
$^{238}{ m U}$	0.0018	0.088	0.38	1.7
$^{232}\mathrm{Th}$	0.0004	4.63	0.51	2.74
$^{40}{ m K}$		0.09	4	13.95
60 Co			0.2	1.03
¹³⁷ Cs			0.16	2.36
$^{222}\mathrm{Rn}$	$10~\mu\mathrm{Bq}\cdot\mathrm{m}^{-3}$			
³⁹ Ar	10^{3}			

as lithographed copper mesh, avalanche holes, and underlining PCB patterns. Surface contaminations of Microbulk Micromegas were measured and we use the measurement value without implementing a detailed structure. The structure was substituted with a 0.1 mm thick copper. The readout plane on the top of the sensitive volume consists of 6 Micromegas modules and is 58.0 cm long and 38.5 cm wide. The cathode made of 2 mm thick oxygen-free copper has the same surface area and is facing the readout plane beneath the sensitive volume. A 4 cm thick acrylic frame surrounding the sensitive volume from four sides represents the mechanical structure of the field cage and acrylic frame. We put a $55\times35\times0.01$ cm³ sample on the cathode in the simulation. All the components described above are enclosed in a 1 cm thick SS vessel with an inner volume of $80\times60\times15$ cm³.

We simulate major background contributions from surface and bulk containments of all components. The energy deposition process of $\alpha,\,\beta,$ and γ particles in the TPC are simulated with Geant4. For the study of α contaminations on the sample surface, we expect the β and γ background events from detector bulk material have a marginal impact. We confirm this in our simulation first before focusing on α background from surfaces of detector components.

Major bulk background sources such as 238 U, 232 Th, and other radio-contaminations in different materials are listed in Table 1. Radio-contamination of oxygen-free copper and SS follows measurements of the PandaX Collaboration [12]. For acrylic, the radioactivities are assumed to be the same as what is used by JUNO [23]. The working gas medium is argon for α contamination measurement. The radio-purity of commercial argon gas varies significantly from different vendors or even different batches of the same vendor. For the 238 U and 232 Th in argon, we adopted values from GERDA [24]. Besides, atmospheric argon contains approximately 1 Bq·kg $^{-1}$ of cosmogenic 39 Ar [25], which is a concern for β measurement but will not introduce background in high energy region for α measurement.

 ^{222}Rn in argon is listed separately from the parent ^{238}U chain. Radon is a noble gas and is usual in $\mu\text{Bq-mBq-m}^{-3}$ level in commercial argon gas supply. The contamination can be reduced by at least three orders of magnitude after passing through an activated carbon cold trap [26]. We assumed a concentration of ^{222}Rn of 10 $\mu\text{Bq}\cdot\text{m}^{-3}$ in our simulations.

Fig. 6 shows the energy deposition of β and γ events in Screener3D. Due to the relatively small dE/dx of β and γ , the typical energy deposition is less than 1 MeV, which is distinctively different from that of α particles. Therefore, we define the region of interest (ROI) for α particle measurement above 1 MeV. The upper limit for α ROI is 10 MeV, which is above the highest α energy of naturally occurring radioactivities of the decay chains of uranium and thorium.

Only α -emitting surface directly facing the sensitive volume, including argon gas, readout plane, field cage, and cathode contribute to the α background. α particles with energy below 10 MeV travel less than 20 μ m in copper and less than 100 μ m in acrylic. Therefore, α contaminations near the surface are our main focus. The concentration of α -emitting radio-isotopes, especially decay chains of 238 U and 232 Th,

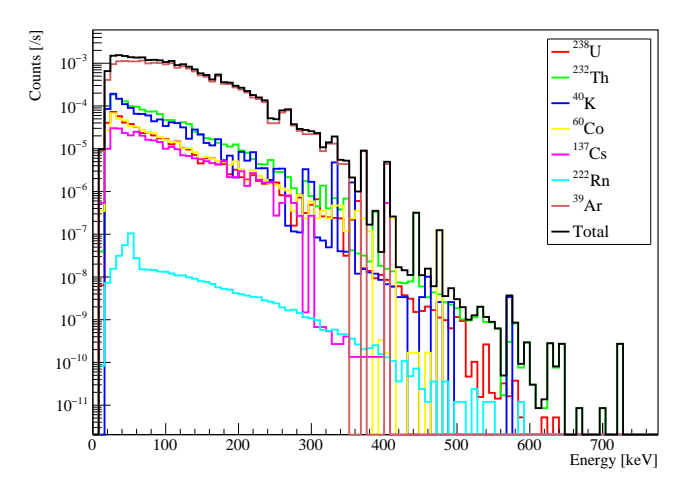


Fig. 6. Low energy spectra of Screener3D. Main contributions in the energy range are from γ and β .

Table 2. Radioactivity level of surface in Screener3D $(mBq \cdot m^{-2})$

Material	Acrylic	Oxygen-free copper	Readout plane
²³⁸ U	0.25	1.30	0.45
²³² Th	0.08	1.30	0.14

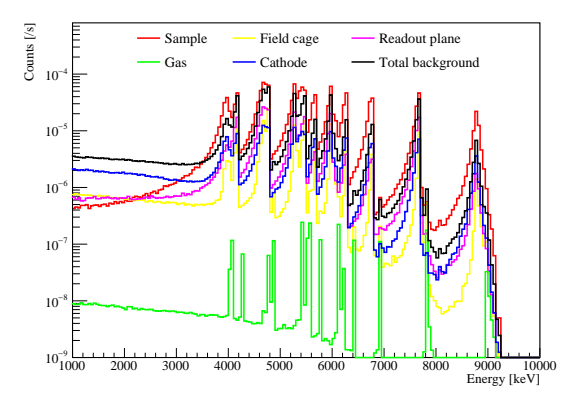
on the surface is usually higher than that in the bulk, due to secondary contamination. The surface radioactivities of acrylic, oxygen-free copper, and Micromegas readout plane are shown in Table 2. We deduced a conservative surface contamination level of acrylic from JUNO Collaboration's measurements. JUNO reported the acrylic contamination level with and without the surface cleaning with Alconox solution [27]. For copper, we adopt the maximum values measured by the CUORE Collaboration in dedicated bolometer arrays [28]. The radioactivity levels of the readout plane follow the results of Microbulk Micromegas measured by the BiPo-3 detector [21].

The depth profile of surface contaminations can be approximated by an exponential curve,

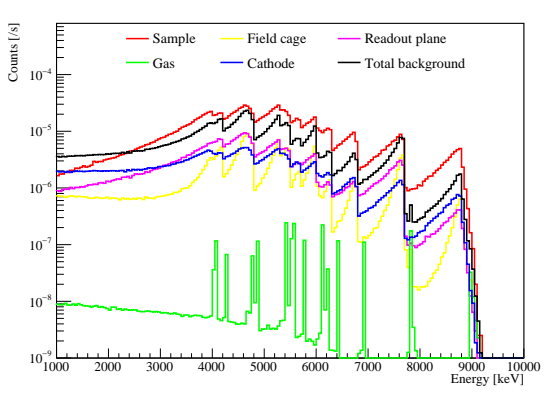
$$\rho = \rho_0 e^{-\frac{x}{\lambda}} + b,\tag{1}$$

where ρ_0 is the surface contamination per unit volume at the very surface, x is the distance into the bulk material, λ is the characteristic penetration depth of the contamination, and b is the contamination level in the bulk material. At the very surface, the contamination level is ρ_0+b . λ may vary greatly with the contamination type and causes of the contaminations. Verification of the depth profile and pinpointing the exact value of λ can be done by measuring the peak shape of α spectrum but are challenging experimentally. In our simulation, we set $\lambda=0.1~\mu\text{m}$, which is a shallow distribution but the effects can still be experimentally identified. At the same time, we compared our results with $\lambda=1~\mu\text{m}$, to study the influence of the penetration depth of the contamination. For both λ values, the total amount of the surface contaminations in the materials is the same.

Fig. 7 shows energy spectra of a copper sample on the cath-



(a) Geant4-simulated energy spectra assuming $\lambda=0.1\,\mu\mathrm{m}$.



(b) Geant4-simulated energy spectra assuming $\lambda=1~\mu\mathrm{m}$.

Fig. 7. Geant4-simulated energy spectra of Screener3D. For a longer penetration depth of $\lambda=1~\mu\text{m}$, α particles are more likely to lose partial energy before escaping the surface. Therefore, the tail of the characteristic peak is more obvious in figure (b).

ode plane and different detector components for both λ values. The count rates of the sample, field cage, readout plane, and cathode are scaled with the surface area and the corresponding surface radioactivity level listed in Table 2. For the gas medium, the spectrum is determined by the contamination level of radon and total argon mass. The bulk radioactivity level used in the simulation is listed in Table 1.

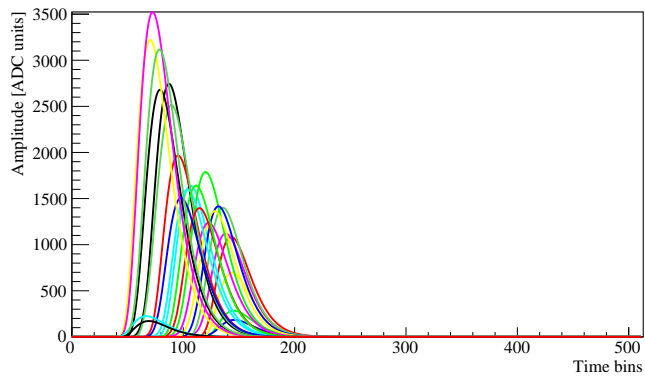
In the ROI between 1 and 10 MeV, the total expected background rate is 82.4 (76.1) counts per day for $\lambda=0.1\,\mu\mathrm{m}$ (1 $\mu\mathrm{m}$). About 46.0% (45.4%) of the background is from the readout plane, 36.1% (35.8%) of the background from the cathode, 17.6% (18.5%) of the background from the field cage, and 0.3% (0.3%) of the background from the working gas. The difference in α peak shapes of Fig. 7 (a) and Fig. 7 (b) highlight the impact of depth profile. For relatively radioactive samples with high contamination levels, we can potentially have a quantitative estimation of the depth profile. In the two figures, the spectra from argon gas are identical.

B. Detector response simulation

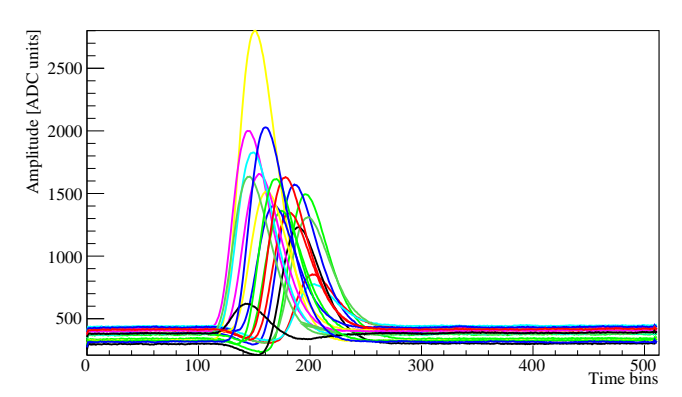
Detector response, including electron diffusion, energy resolution, readout scheme, and electronics response, is added to Geant4 simulation data to produce mock detector data for downstream analysis. The detector response is simulated with the REST framework [29], which is developed and used by PandaX-III [30] and other gas TPC projects. If we take an α particle traveling in gas as an example, Geant4 records the differential energy deposition dE/dx along the trajectory. In REST, the differential energy deposition is converted to the number of ionization electrons in gas. The ionization electrons diffuse while drifting to the readout plane. REST interfaces with the Garfield program [31] to calculate diffusion coefficients. For argon/isobutane(5%) mixture at 1 bar and under an electric field of 100 V/cm, the transverse (longitudinal) diffusion coefficient is 0.048 (0.044) $\sqrt{\text{cm}}$. Once the diffused electrons reach the readout plane, the position and arrival time are recorded. Following the strip-readout schemes of Micromegas in the actual detectors, ionization electrons are grouped by strips, and pulses are generated strip by strip, as shown in Fig. 8 (a). Colored pulses represent signals from different strips. Pulse amplitude in Fig. 8 is proportional to the number of electrons collected per strip. The amplitudes are smeared according to a Gaussian function to account for an energy resolution of 3% full width half maximum (FWHM) at 2.5 MeV in the detector response simulation. Pulse widths are determined from electronics shaping and a 1 μ s shaping time is used in Fig. 8 (a). The relative timing among pulses indicates the arrival time of electrons. Under a relative constant drift velocity of approximately 30 mm/ μ s, the arrival time denotes the relative energy deposition position in the drift direction. For a sampling rate of 50 MHz and a record length of 512 sample points per signal, we record approximately 10 μ s of data per signal window. For a drift length of 10 cm in our TPC, the signal window is more than adequate, as shown in the figure. We also implemented triggers in REST, but the trigger threshold effect is negligible for α events in the ROI.

For comparison, Fig. 8 (b) is an α event recorded by a gaseous detector. The detector is equipped with a $20 \times 20 \text{ cm}^2$ Micromegas and filled with 1 bar of argon and 5% isobutane gas mixture. The height of the drift volume is 10 cm, the same as in our simulation. As we can see, our mock pulses reproduce the key features of detector pulses. Next, the mock pulses of each simulated event are analyzed using the same procedure as detector data.

Energy is reconstructed with mock pulses and the resulting spectra are shown in Fig. 9. Compared to Fig. 7, the α peaks are broadened due to the detector resolution. Since the effective area of the readout plane does not cover the full area of the field cage, partial energy of background events from the field cage will not be recorded. Therefore, the spectrum of background events from the field cage shifts to lower energy compared to that in Fig. 7. Meanwhile, a small peak is shown in front of some characteristic peaks from the readout plane.



(a) Simulated waveforms recorded by Micromegas



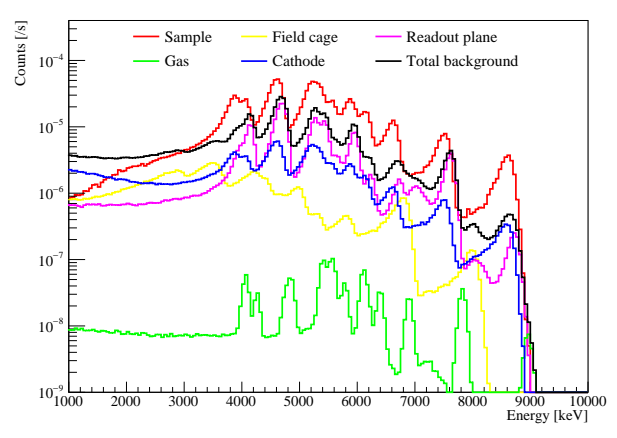
(b) Measured waveforms of an α event in a TPC with a Microbulk Micromegas readout plane.

Fig. 8. Simulated (a) and measured (b) waveforms of an α event. The measurement was done with 1 bar of argon and 5% isobutane gas mixture.

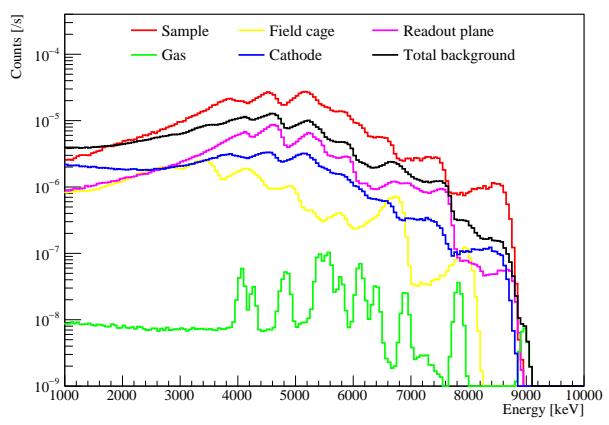
C. Track reconstruction

The main application of mock pulses is track reconstruction. As mentioned earlier, the amplitude and timing of pulses of different strips contain all the information we would collect from a real detector. Therefore, this information can be used to reconstruct the particle tracks and differential energy loss along the tracks in a TPC. Track reconstruction is done in XZ and YZ planes, where Z denotes the drift direction and X/Y represents transverse directions. In 1 bar argon, α particles would rarely be scattered by a large angle and the tracks are mostly straight. Fig. 10 (a) shows an α track in the XZ and YZ planes. The red trace represents the trajectory and yellow dots represent the energy deposition vertex. The size of yellow dots illustrates the relative amount of energy deposition. The Bragg peak is prominent at the end of the trajectory on the top left of the figures.

In Fig. 10 (b), we show the reconstructed track in XZ and YZ planes of the same event as in Fig. 10 (a). Each red (or green) point in the figures represents a triggered strip signal, and the size of the point represents the amount of deposited energy. The X (Y) coordinate is determined from the position of the strip. The Z-axis indicates the position of the ionized electron relative to that of the first electron to reach the



(a) Simulated energy spectra with detector response assuming $\lambda = 0.1 \, \mu \text{m}$.



(b) Simulated energy spectra with detector response assuming $\lambda = 1 \, \mu \text{m}$.

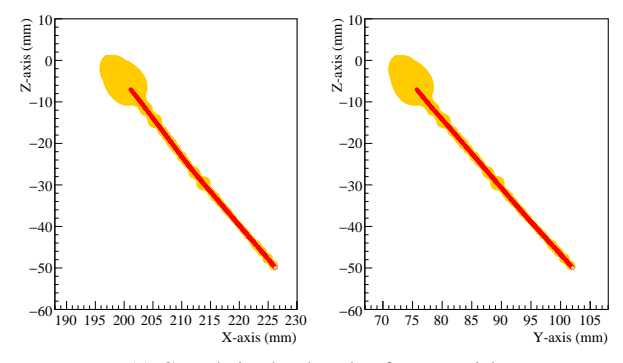
Fig. 9. Simulated energy spectra of Screener3D with detector response added.

readout plane, as determined by the drift velocity and pulse timing. For long, near-straight α tracks, sorting by timing or X/Y position can reliably reconstruct the true tracks. The black lines in Fig. 10 (b) represent a well-reconstructed track. Track reconstruction can be challenging when the tracks are short. For example, the length of the XZ and/or YZ tracks may be very short due to the projection angle. The tracks may also be short when α particles only deposit partial energy in the active volume.

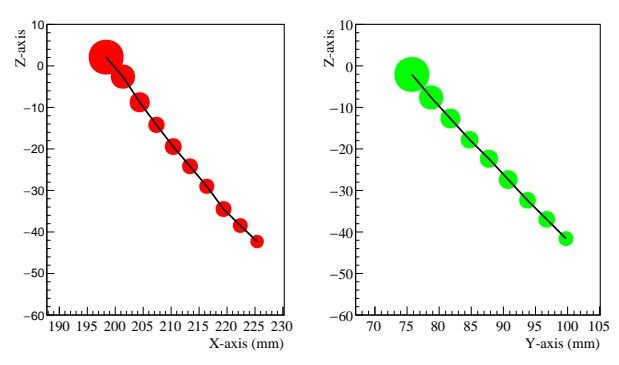
D. Screener3D background suppression

In our region of interest from 1 to 10 MeV for α measurement, effectively all the β/γ background are removed. The ROI cut also removes 11% of α background and keeps 98.9% of the signal events. Alpha background can be further suppressed by a fiducial cut, an angle cut, and a hit-number cut. We will explain the cuts in detail as follows.

We set the cut values to maximize the detector sensitivity S_d . For measurements with a large number of back-



(a) Geant4-simulated tracks of an α particle.



(b) Hits recorded by Micromegas strips and the reconstructed track.

Fig. 10. Geant4-simulated (a) and reconstructed (b) tracks of an α particle. In (a), the straight red line represents the α particle track and yellow dots represent the relative size of energy deposition. In (b), Each red/green dot represents a triggered strip signal and the size of the dot represents the amount of deposited energy in the strip. The black line is the reconstructed track by connecting nearby hits.

grounds B, background fluctuation follows Poissonian distribution and equals to \sqrt{B} . Therefore, the detector sensitivity is proportional to $\epsilon_s/\sqrt{\epsilon_b}$, where ϵ_s is the signal detecting efficiency and ϵ_b is the efficiency that background events are kept by selection cuts. For each cut, we select the cut values that makes the $\epsilon_s/\sqrt{\epsilon_b}$ maximum.

We have devised two competing algorithms to identify the Bragg peak of a track and thus the track's origin as well as direction. A track in the XZ or YZ plane is split into two segments from the mid-point and energy in each segment is calculated. The Bragg peak is more likely to be in the segment with larger energy. The energy of each hit point and dE/dx along the vertical direction can also be used to locate Bragg peaks. When particle energy is higher than 1 MeV and the total hits number is larger than 10, the identify efficiency of the track's direction is about 97%.

We can identify the starting point of each track and the distribution is shown in Fig. 11. The X-axis in the figure is called fiducial distance, which is defined as the distance in the inward direction from the inner surface of the field cage. The majority of the events from the field cage and cathode originate from the edge of the sensitive volume. For those events,

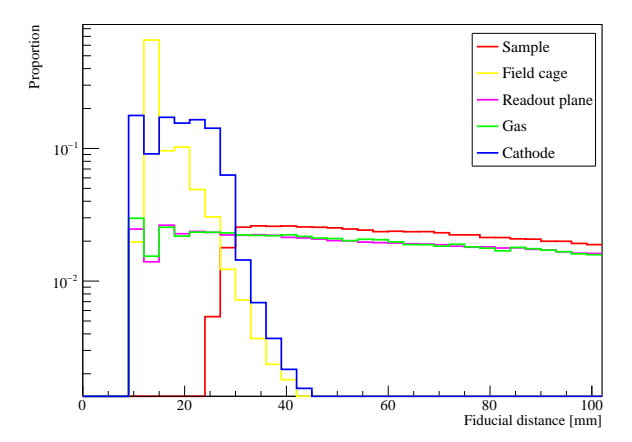


Fig. 11. Distribution of tracks' starting point. We make a cut at the fiducial distance of 27 mm to effectively remove the background events from the field cage and cathode.

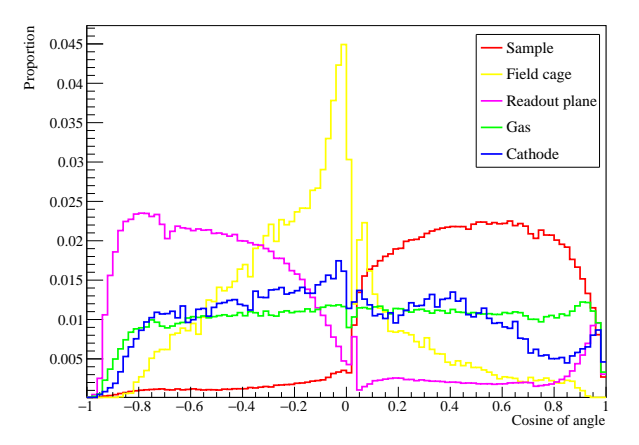


Fig. 12. Distribution of track direction, defined as cosine of the angle between track and vertical direction. We make a cut at 0 to effectively remove the background events from the readout plane and gas.

the fiducial distance is less than 50 mm. We make a fiducial cut at fiducial distance 27 mm and discard any events with a smaller fiducial distance, i.e., closer to the edge of the active volume. After the fiducial cut, the signal efficiency is at 96.2%. Less than 3% of the events from field cage and cathode background remains. The cut is less effective for other background sources and the efficiencies are listed in Table 3.

Fig. 12 shows the distribution of $\cos(\theta)$, where θ is the angle between the particle traveling direction and upward vertical direction. The majority of α events from samples would have positive $\cos(\theta)$ values while events from the readout plane have negative values, as shown clearly in the figure. Events from the sample with negative $\cos(\theta)$ are mostly short events with wrong track reconstruction. The same is true for events from the readout plane but with positive $\cos(\theta)$. We make a cut at 0 and reject events with $\cos(\theta) < 0$. The cut rejects most of the residual background events from the readout

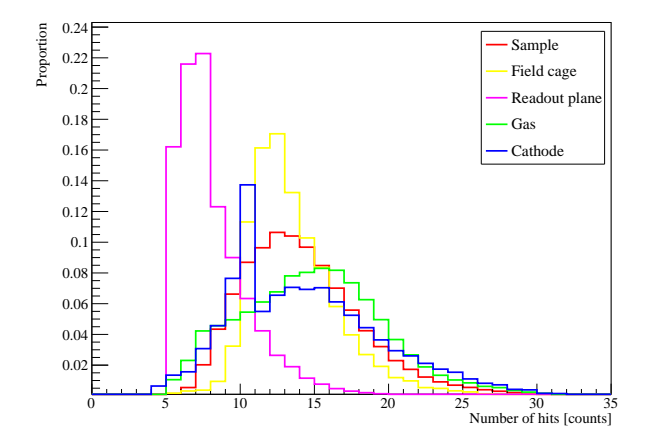


Fig. 13. Distribution of number of hits of an event. We make a cut at 10 (9 when $\lambda=1~\mu{\rm m}$) to remove the events with short tracks.

Table 3. The α background residual rate after each $\mathrm{cut}(\lambda = 0.1 \mu\mathrm{m})$

Cut parameter	Energy	Fiducial	Angle	Hit number
	cut	cut	cut	cut
Field cage	83.9%	2.9%	0.7%	0.5%
Cathode	79.5%	2.7%	1.5%	1.2%
Readout plane	95.1%	80.3%	7.1%	1.2%
Working gas	92.0%	77.1%	40.5%	28.9%
Sample	98.9%	96.2%	92.2%	74.2%

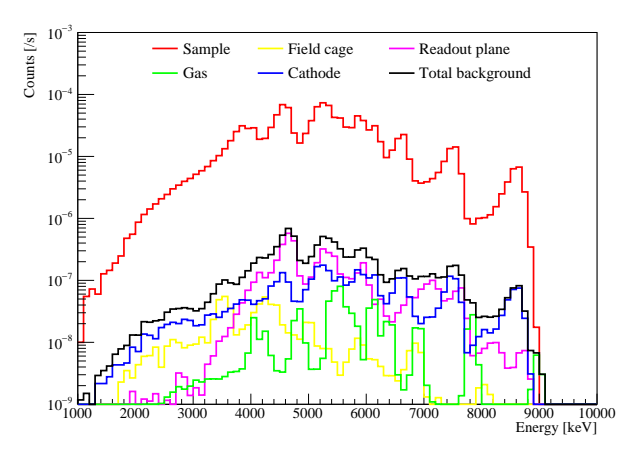
plane and at least 50% of those from the field cage, cathode, and argon gas (see Table 3).

We also count the number of hit strips to further reject background events. Electrons generated by an event from the sample will be diffused while drifting to the readout plane. In 1 bar of argon and 5% isobutane gas mixture, the transversal diffusion is about 1.2 cm in our TPC. Therefore, signals from the sample will trigger four strips at least. The drifting distance for an α event from the readout plane depends on the track length. The short track from the readout plane may trigger a few strips. A triggered strip means a hit point on the track. There is a gap of about 1 cm between the field cage and the readout plane. Tracks in the gap will not be recorded, which results in fewer hit points. The distribution of the hits number is shown in Fig. 13. We only keep events that trigger more than 10 (9 when $\lambda=1~\mu{\rm m})$ strips. The backgrounds are further suppressed.

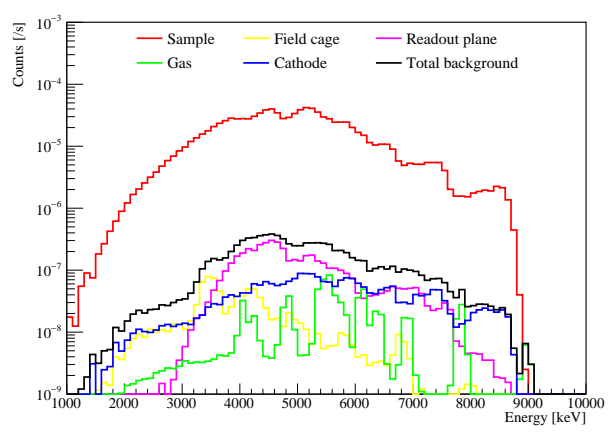
Fig. 14 shows the signal and background spectra after all cuts. The backgrounds are suppressed by nearly two orders

Table 4. The α background residual rate after each $\mathrm{cut}(\lambda = 1 \, \mu \mathrm{m})$

Cut parameter	Energy	Fiducial	Angle	Hit number
	cut	cut	cut	cut
Field cage	83.5%	2.8%	0.7%	0.6%
Cathode	78.7%	2.7%	1.3%	0.9%
Readout plane	94.0%	79.3%	10.1%	1.2%
Working gas	92.0%	77.1%	40.5%	31.3%
Sample	97.0%	94.3%	87.5%	67.9%



(a) Energy spectra after all the cuts assuming $\lambda = 0.1 \, \mu \text{m}$.



(b) Energy spectra after all the cuts assuming $\lambda=1~\mu\mathrm{m}$.

Fig. 14. Energy spectra after all the cuts. The backgrounds are suppressed by nearly two orders of magnitude while nearly 70% signals are preserved.

of magnitude while keeping signal efficiency high. For the $\lambda=0.1\,\mu\mathrm{m}$ case, the combination of all the cuts would reduce α background rate from 82.3 to 0.9 counts per day while keeping 74.2% of the signals. Among the remaining background events, 49.7% comes from the readout plane, 36.5% from the cathode, 7.1% from the field cage, and 6.7% from the gas. Assuming $\lambda=1\,\mu\mathrm{m}$, the background is suppressed from 76.1 to 0.8 counts per day while 67.9% of the signal is preserved. About 52.5% of the remaining background comes from the readout plane, 28.7% from the cathode, 10.2% from the field cage, and 8.6% from the gas. Due to more α events generating below the surface and thus lose partial energy before they are emitted from the surface, both the total residual events of background and signal is slightly fewer than that of the $\lambda=0.1\,\mu\mathrm{m}$.

Table 5. Sensitivities of Screener3D for total α measurement (the results in parentheses from λ =1 μ m).

Measurement time	Bckground events	Sensitivity
(day)	(counts)	$(\mu \mathrm{Bq}\cdot\mathrm{m}^{-2})$
1	0.93 (0.79)	149 (153)
2	1.86 (1.59)	97 (99)
7	6.50 (5.56)	46 (47)

Table 6. Sensitivities of Screener3D for α measurement from polonium (the results in parentheses from λ =1 μ m)

Nuclide	Background events	Sensitivity
	(counts)	$(\mu \mathrm{Bq}\cdot\mathrm{m}^{-2})$
²¹² Po	0.03(0.02)	42(36)
²¹⁴ Po	0.89(0.05)	54(47)

E. Screener3D measurement sensitivity

Assuming no events are observed from the samples statistically different from the fluctuation of background, we can evaluate the sensitivity of Screener3D for a given screening period T in days. With a background rate of R_{bkg} counts per day, the total background for a measurement is $B=R_{bkg}T$. We use the Poissonian fluctuation of small background values to calculate the upper limit on counts and subsequent surface background rate. For small B and a Confidence Level (C.L.) of Γ , the upper limit for counts of signal \hat{S} can be expressed as [32]

$$\sum_{k=\hat{S}+B}^{\infty} p_B(k) = 1 - \Gamma \tag{2}$$

 \hat{S} can be evaluated numerically or with a lower incomplete Gamma function. Lastly, the sensitivity can be calculated with the signal efficiency, \hat{S} , and sample surface areas. Table 5 shows the sensitivity of Screener3D with typical measurement periods. We can reach a sensitivity of 97 μ Bq·m⁻² at the 90% C.L. for a two-day measurement, assuming a typical sample such as copper and an exponential surface contamination profile with $\lambda=0.1\,\mu$ m. The sensitivity would be better than 50 μ Bq·m⁻² when the measurement duration is extended to one week. For a characteristic depth $\lambda=1\,\mu$ m, the results are very similar, as shown in Table 5.

The Screener3D can also measure α rates of a specific nuclide, such as 212 Po of the thorium decay chain and 214 Po of the uranium decay chain. The signature α peak of 212 Po is at 8.8 MeV and we define a specific ROI between 8 and 9 MeV In the ROI, 7% of background events and 98% of

the signals are reserved after the energy and topology cuts. The final background rate is 0.03 (0.02 when $\lambda = 1 \mu \rm m)$ counts per day. The corresponding sensitivity for $^{212}\rm{Po}$ is 42 (or 36 when $\lambda = 1 \mu \rm m)~\mu \rm Bq \cdot m^{-2}$ after one-day measurement. For $^{214}\rm{Po}$ in the ROI of 7 and 8 MeV, 97% of the background is removed while 98% of the signals has remained. The final background rate is 0.09 (0.05 when $\lambda = 1 \mu \rm m)$ counts per day. The sensitivity is 54 (47 when $\lambda = 1 \mu \rm m)~\mu \rm Bq \cdot m^{-2}$ for one-day measurement.

IV. SUMMARY AND OUTLOOK

Background events from detector surfaces may have a severe negative impact on rare event search experiments. Screening methods for surface contaminations have not been utilized as widely as gamma spectrometer and mass spectrometer for bulk contaminations. In this work, we propose a charged particle detector using the TPC concept for surface contamination screening. The TPC design concept and detector background control are described in detail. In addition, the Screener3D can significantly reduce α background rate from itself by topological characteristics of particle trajectories, a unique feature of the gaseous detector. Eventually, we can have a detector with fewer than one α background count per day. With a large active area of approximately 2000 cm², we reach a sensitivity of better than $100 \mu \text{Bq} \cdot \text{m}^{-2}$ for surface α contaminations with two days of measurements. If we only counter α particles from specific α peaks, the sensitivity will be further improved.

Screener3D is currently designed for surface α particles screening mainly and the ROI is typically above 1 MeV. We can also adopt the detector for surface β counting in the energy range of below 1 MeV. However, in the energy range, γ -rays from the detector and nearby laboratory environment are the dominating background. A γ -shielding facility is therefore needed and currently in design. We are also working on the track reconstruction algorithms to better reconstruct the more meandering β tracks, aiming to locate the starting position with high precision. Screening capability for surface β will be reported in a future manuscript.

V. ACKNOWLEDGEMENTS

This work is supported by the grant from the Ministry of Science and Technology of China (No. 2016YFA0400302) and the grants from National Natural Sciences Foundation of China (No. 11775142 and No. U1965201). We thank the support from the Chinese Academy of Sciences Center for Excellence in Particle Physics (CCEPP).

 ^[1] S. DellOro, S. Marcocci, M. Viel et al, Neutrinoless double beta decay:2015 review. Adv. High Energy Phys 2016, 2162659 (2016). http://dx.doi.org/10.1038/10.1155/2016/2162659

^[2] L. Roszkowski, E.M. Sessolo, and S. Trojanowski, WIMP dark matter candidates and searches-current status and fu-

ture prospects. Rept. Prog. Phys **81(6)**, 066201 (2018). http://dx.doi.org/10.1088/1361-6633/aab913

^[3] J. Liu, X. Chen, and X. Ji, Current status of direct dark matter detection experiments. Nature Phys 13(3), 212–216 (2017). http://dx.doi.org/10.1038/nphys4039

- [4] J.-P. Cheng, K.-J. Kang, J.-M. Li et al, The China Jinping Underground Laboratory and its Early Science. Ann. Rev. Nucl. Part. Sci 67,231–251 (2017). http://dx.doi.org/10.1146/annurev-nucl-102115-044842
- [5] N. Abgrall, I.J. Arnquist, F.T. AvignoneIII, et al, The Majorana Demonstrator radioassay program. Nucl. Instrum. Meth A,828, 22–36 (2016). http://dx.doi.org/10.1016/j.nima.2016.04.070
- [6] D.S. Akerib, H.M. Araújo, X. Bai, et al, Radiogenic and Muon-Induced Backgrounds in the LUX Dark Matter Detector. Astropart. Phys 62,33–46 (2015). http://dx.doi.org/10.1016/j.astropartphys.2014.07.009
- [7] F. Alessandria, E.Andreotti, R.Ardito et al, CUORE crystal validation runs: results on radioactive contamination and extrapolation to CUORE background. Astropart. Phys 35, 839–849 (2012). http://dx.doi.org/10.1016/j.astropartphys.2012.02.008
- [8] H. Jiang, L.P. Jia, Q. Yue, et al, Limits on Light Weakly Interacting Massive Particles from the First 102.8 kg x day Data of the CDEX-10 Experiment. Phys. Rev. Lett 120(24),241301 (2018). http://dx.doi.org/10.1103/PhysRevLett.120.241301
- [9] D.S. Leonard, P. Grinberg, P. Weber, et al, Systematic study of trace radioactive impurities in candidate construction materials for EXO-200. Nucl.Instrum. Meth. A 591, 490–509 (2008). http://dx.doi.org/10.1016/j.nima.2008.03.001
- [10] X. Wang, X. Chen, C. Fu et al, Material Screening with HPGe Counting Station for PandaX Experiment. JINST 11(12),T12002 (2016). http://dx.doi.org/10.1088/1748-0221/11/12/T12002
- [11] C. Alduino, K. Alfonso, D.R. Artusa, et al, Measurement of the two-neutrino double-beta decay half-life of ¹³⁰Te with the CUORE-0 experiment. Eur. Phys. J. C **77(1)**, 13 (2017). http://dx.doi.org/10.1140/epjc/s10052-016-4498-6
- [12] H. Zhang, H.G. Zhang, A. Abdukerim, et al, Dark matter direct search sensitivity of the PandaX-4T experiment. Sci. China Phys. Mech. Astron 62(3), 31011 (2019). http://dx.doi.org/10.1007/s11433-018-9259-0
- [13] Ortec detectors. https://www.orteconline.com/products/radiation-detectors/
- [14] P.Loaiza, A.S. Barabash, A. Basharina-Freshville, et al, The BiPo-3 detector. Appl. Radiat. Isot123, 28242294(2017). https://doi.org/10.1016/j.apradiso.2017.01.021
- [15] XIA Ultralo 1800 gas counter. https://xia.com/ultralo.html
- [16] R. Bunker, et al. The BetaCage, an Ultra-Sensitive Screener for Surface Contamination. AIP Conference Proceedings **1549**, 132–35 (2013). https://doi.org/10.1063/1.4818093
- [17] H. Ito, et al, Development of an Alpha-Particle Imaging Detector Based on a Low Radioactive Micro-Time-Projection Chamber. Nucl. Instrum. Meth. A. 953, 163050 (2020). https://doi.org/10.1016/j.nima.2019.163050
- [18] S. Andriamonje, D. Attie, E. Berthoumieux at el, Development and performance of Microbulk Micromegas detectors. Journal of Instrumentation 4, 02001(2010).

- https://doi.org/10.1088/1748-0221/5/02/p02001
- [19] COMSOL. https://www.comsol.com
- [20] X. Yan, X. Chen, Y. Chen, et al, Slow Control System for PandaX-III experiment. JINST16(05),T05004 (2021). https://doi.org/10.1088/1748-0221/16/05/t05004
- [21] J. Castel, I. Coarasa, T. Dafni, et al, Background assessment for the TREX dark matter experiment. Eur. Phys. J. C. 79, 782 (2019). https://doi.org/10.1140/epjc/s10052-019-7282-6
- [22] S. Agostinelli, J. Allison, K. Amako, et al, (GEANT4 Collaboration), GEANT4: A Simulation toolkit. Nucl. Instrum. Meth. A. 506, 250 (2003). https://doi.org/10.1016/S0168-9002(03)01368-8
- [23] X. Fang, Y. Zhang, G.H. Gong, et al, Capability of detecting low energy events in JUNO Central Detector. JINST 15, P03020 (2020). https://doi.org/10.1088/1748-0221/15/03/P03020
- [24] D. Budjá, A.M. Gangapshev, J. Gasparro, et al, Gammaray spectrometry of ultra low levels of radioactivity within the material screening program for the GERDA experiment. Applied Radiation and Isotopes 67(5), 755 – 758(2009). http://dx.doi.org/10.1016/j.apradiso.2009.01.019
- [25] P. Agnes, L. Agostino, I.F.M. Albuquerque, et al, Results From the First Use of Low Radioactivity Argon in a Dark Matter Search. Phys. Rev. D 93(8),081101, (2016). http://dx.doi.org/10.1103/PhysRevD.93.081101
- [26] H. Simgen, and G. Zuzel, Analysis of the ²²²Rn concentration in argon and a purification technique for gaseous and liquid argon. Appl Radiat Isot. **67(5)**, 922-5(2009). http://dx.doi.org/10.1016/j.apradiso.2009.01.058. Epub 2009 Jan 25. PMID: 19251429
- [27] C.Y. Cao, N. Li, X.Y Yang at el, A practical approach of high precision U and Th concentration measurement in acrylic. Nucl. Instrum. Meth. A 1004, 165377(2021). https://doi.org/10.1016/j.nima.2021.165377
- [28] F. Alessandria, R. Ardito, D.R. Artusa at el, Validation of techniques to mitigate copper surface contamination in CUORE. Astroparticle Physics 45, 13-22(2013). https://doi.org/10.1016/j.astropartphys.2013.02.005
- [29] J. Galan, X. Chen, H. Du, et al, Topological background discrimination in the PandaX-III neutrinoless double beta decay experiment, J. Phys. G: Nucl. Part. Phys. 47, 045108 (2020). https://doi.org/10.1088/1361-6471/ab4dbe
- [30] X. Chen, C.B. Fu, J. Galan, et al, PandaX-III: Searching for neutrinoless double beta decay with high pressure ¹³⁶Xe gas time projection chambers. China Phys. Mech. Astron **60(6)**, 061011 (2017). http://dx.doi.org/10.1007/s11433-017-9028-0
- [31] R. Veenhof, Garfield simulation of gaseous detectors. http://garfield.web.cern.ch/garfield/
- [32] F. Alessandria, R. Ardito, D. R. Artusa, et al, Sensitivity of CUORE to Neutrinoless Double-Beta Decay. arXiv v3, (2013). https://arxiv.org/abs/1109.0494v3